J. Fluid Mech. (2012), *vol.* 694, *pp.* 332–351. © Cambridge University Press 2012
doi:10.1017/jfm.2011.549

Dissipation element analysis in turbulent channel flow

Fettah Aldudak[1]† **and Martin Oberlack**[1,2,3]

[1] Department of Mechanical Engineering, TU Darmstadt, Petersenstrasse 30, 64287 Darmstadt, Germany

[2] Center of Smart Interfaces, TU Darmstadt, Petersenstrasse 32, 64287 Darmstadt, Germany

[3] GS Computational Engineering, TU Darmstadt, Dolivostrasse 15, 64293 Darmstadt, Germany

(Received 13 December 2010; revised 10 November 2011; accepted 5 December 2011; first published online 2 February 2012)

In order to analyse the geometric structure of turbulent flow patterns and their statistics for various scalar fields we adopt the dissipation element (DE) approach and apply it to turbulent channel flow by employing direct numerical simulations (DNS) of the Navier–Stokes equations. Gradient trajectories starting from any point in a scalar field $\phi(x, y, z, t)$ in the directions of ascending and descending scalar gradients will always reach an extremum, i.e. a minimum or a maximum point, where $\nabla\phi = 0$. The set of all points and trajectories belonging to the same pair of extremal points defines a dissipation element. Extending previous DE approaches, which were only applied to homogeneous turbulence, we here focus on exploring the influence of solid walls on the dissipation element distribution. Employing group-theoretical methods and known symmetries of Navier–Stokes equations, we observe for the core region of the flow, i.e. the region beyond the buffer layer, that the probability distribution function (p.d.f.) of the DE length exhibits an invariant functional form, in other words, self-similar behaviour with respect to the wall distance. This is further augmented by the scaling behaviour of the mean DE length scale which shows a linear scaling with the wall distance. The known proportionality of the mean DE length and the Taylor length scale is also revisited. Utilizing a geometric analogy we give the number of DE elements as a function of the wall distance. Further, it is observed that the DE p.d.f. is rather insensitive, i.e. invariant with respect both to the Reynolds number and the actual scalar ϕ which has been employed for the analysis. In fact, a very remarkable degree of isotropy is observed for the DE p.d.f. in regions of high shear. This is in stark contrast to classical Kolmogorov scaling laws which usually exhibit a strong dependence on quantities such as shear, anisotropy and Reynolds number. In addition, Kolmogorov's scaling behaviour is in many cases only visible for very large Reynolds numbers. This is rather different in the present DE approach which applies also for low Reynolds numbers. Moreover, we show that the DE p.d.f. agrees very well with the log-normal distribution and derive a log-normal p.d.f. model taking into account the wall-normal dependence. Finally, the conditional mean scalar differences of the turbulent kinetic energy at the extremal points of DE are examined. We present a power law with scaling exponent of $2/3$ known from Kolmogorov's hypothesis for the centre of the channel and a logarithmic law near the wall.

Key words: Turbulence, channel flow, length scales, dissipation element, DNS

† Email address for correspondence: aldudak@fdy.tu-darmstadt.de

https://doi.org/10.1017/jfm.2011.549 Published online by Cambridge University Press

1. Introduction

Wall-bounded turbulent flows exhibit certain characteristic regions in the wall-normal direction, based e.g. on the functional form of the mean profile, where different turbulence phenomena are dominant to different degrees. Hence, all statistical quantities of these flows are inhomogeneous in the wall-normal direction. For the present case of a pressure-driven turbulent channel flow four layers exist: a viscosity-dominated sublayer, a buffer layer where production of turbulent kinetic energy and the turbulence intensity itself reach their maximum, a logarithmic layer where production and dissipation are of the same order of magnitude and a core region, often denoted the defect layer (Pope 2000).

Because of the fact that, in fully developed wall turbulence sufficiently far from the wall (i.e. in the log-layer and beyond) and for scales considerably larger than the Kolmogorov length scale, inertial forces dominate the viscous forces and, hence, the turbulent stresses are significantly larger than the viscous stresses, one can neglect the influence of the viscous forces on the large scales. Thus, the velocity scaling is assumed to be independent of viscosity.

A significant phenomenon in turbulence is the energy transfer among different turbulent length scales. There is a wide spectrum of length scales in turbulent flows which are limited by the spatial dimensions of the flow field from above and by the Kolmogorov scale from below. In the region far from the largest and the smallest scales local motions are largely independent of boundary influences and viscosity. Among these scales the integral length scale is an estimate of the largest turbulent scales and corresponds to the size of the largest eddies which are usually anisotropic and of the order of the channel height in our case. Since the characteristic velocity of these eddies is of the same order of magnitude as the mean fluid velocity, their Reynolds number is large and the direct effect of the viscosity can be neglected in a statistical sense. Richardson's concept of the energy cascade (Richardson 1922) postulates that large eddies will break up due to their instability, and transfer their energy to smaller eddies until a stage of small and statistically stable scales is reached. According to Kolmogorov's theory, velocity scales decrease as length scales decrease (Kolmogorov 1941). The postulation is that for any sufficiently large Reynolds number any turbulent flow approaches this universal stage at small scales. At the Kolmogorov scale η the molecular viscosity becomes dominant and the turbulent kinetic energy is dissipated. The Kolmogorov length scale is defined as

$$\eta = \left(\frac{\nu^3}{\epsilon}\right)^{1/4} \quad \text{with } \epsilon = \frac{1}{2}\nu\left(\frac{\partial u_i}{\partial x_j} + \frac{\partial u_j}{\partial x_i}\right)^2, \tag{1.1}$$

ν being the kinematic viscosity and ϵ the energy dissipation rate.

Obukhov (1962) and Corrsin (1951) independently extended the second Kolmogorov hypothesis to the process of turbulent scalar mixing, assuming that many aspects of turbulence are universal, although the application to the passive scalar is complicated by the effects of Prandtl number $Pr = \nu/D$, where D is the molecular diffusivity of the scalar.

Considering pure hydrodynamic turbulence we have an intermediate length scale, the Taylor scale λ, with $\eta \ll \lambda \ll L$. For isotropic turbulence λ is defined by

$$\epsilon = 15\nu\frac{u'^2}{\lambda^2}, \tag{1.2}$$

https://doi.org/10.1017/jfm.2011.549 Published online by Cambridge University Press

where u' is the r.m.s. value of velocity fluctuation. At the same time, this is also a good qualitative measure for anisotropic turbulence since the contribution of the anisotropic part is very small. From this expression one can obtain $\lambda = (10\nu k/\epsilon)^{1/2}$, where $k = (3/2)u'^2$ is the turbulent kinetic energy associated with large-scale eddies. Although the Taylor scale has no distinct physical interpretation, it can be considered as the distance that a large eddy advects a small Kolmogorov eddy during its turnover time $t_\eta = (\nu/\epsilon)^{(1/2)}$.

A rather different but complementary way to classify and characterize turbulent structures is to examine critical points of the turbulent field. Gibson (1968) was the first to analyse in detail these properties and the behaviour of points with zero gradient and minimal gradient surfaces in a passive scalar ϕ in a turbulent field. His motivation was to obtain physical and geometrical information about the smallest scales and their features in a turbulent scalar field. These are primarily determined by the number and distribution of critical points where the scalar gradient vector vanishes, i.e

$$\nabla\phi \equiv 0. \tag{1.3}$$

Gibson (1968) also analysed the mechanism by which extremal points are generated. Convective motion alone is unable to generate extremal points, since without diffusion isoscalar surfaces in a turbulent field will usually follow the fluid motion. Only a diffusion velocity of the same magnitude as the local convective velocity is able to restore the isoscalar surfaces and to generate extremal points (Wang & Peters 2006). From the conclusion that in scalar turbulent fields the local convective velocity is of the order of the Kolmogorov velocity, and equating it with the balancing diffusive velocity, Gibson (1968) concluded that extremal points are generated at scales of the Obukhov–Corrsin length.

Furthermore, Gibson (1968) supposed that the production of zero-gradient points by direct distortion in regions of uniform scalar gradient is due only to eddies larger than the Obukhov–Corrsin scale. For the case $Pr \gg 1$, the latter conclusion implies that any scale in the turbulent field is capable of generating new extremal points from regions of uniform scalar gradient since those length scales are the smallest. If $Pr \ll 1$, the Obukhov–Corrsin length scale is larger than the Kolmogorov length scale. Then, at the level of smallest scales, velocity perturbations are too weak to generate new zero-gradient points.

Gibson concluded that the dominant physical mechanism by which turbulence produces the small-scale features of scalar fields is the local stretching of small-gradient regions. This mechanism should equally apply to strongly diffusive scalars, where the scalar diffusivity is much larger than the viscosity, as well as to weakly diffusive scalars, where the viscosity is much larger than the scalar diffusivity. Considering a one-dimensional model problem, he pointed out that the number of maximum and minimum points must be equal whereas in two dimensions their sum equals the number of saddle points.

In three dimensions no theory is available but in the present direct numerical simulation (DNS) data we found that the numbers of maximal and minimal points are of the same order of magnitude for a turbulent channel flow as shown in a companion publication (Aldudak & Oberlack 2009). However, a simple relation between critical points does not exist.

The present work is inspired by the work of Gibson and Peters (Gibson 1968; Peters & Wang 2006; Wang & Peters 2006) who analysed the small-scale statistics from passive scalar fields of homogeneous shear turbulence obtained from DNS by means of the dissipation element (DE) method. The notion refers to the tracking of gradient

https://doi.org/10.1017/jfm.2011.549 Published online by Cambridge University Press

trajectories starting from every point in the directions of ascending and descending scalar gradients until local minimum and maximum points of the fluctuating scalar field are found. The set of all points which lie on the gradient trajectories leading to the same pair of extremal points defines a dissipation element. To uniquely parameterize the geometry of a dissipation element the Euclidean distance l between its extremal points and the absolute value of the scalar difference $\Delta\phi$ at these two points are chosen. DE are space-filling which means that any turbulent scalar field can be completely decomposed into such elements. This allows the reconstruction of certain statistical quantities of turbulence, being rather different from classical length scale concepts in turbulence theory such as based on Kolmogorov or integral length scales.

Although these spatial structures are far from being regularly shaped, the choice of the above-mentioned parameters is reported to be appropriate by Wang & Peters (2006). The authors postulate an integro-differential evolution equation for the marginal probability density function (p.d.f.) assuming a Poisson process for the cutting of linear elements and a reconnection process due to molecular diffusion. The conditional mean of the scalar difference is shown to closely follow the inertial-range Kolmogorov scaling over a large range of length scales. Later, they found (see Wang & Peters 2008) that while the conditional mean difference follows the inertial-range Kolmogorov scaling for the passive scalar field, this is not the case for the components of the velocity. The authors trace this back to the imposed high shear rate of the DNS calculations and to the fact that the velocity field might be not fully isotropic.

In the latter work, the dissipation element methodology is extended to other fields in turbulence. The length-scale distribution function for various turbulent fields is compared with the model equation. From their findings they concluded that the mean distance between extremal points, which corresponds to the mean length of the dissipation elements, is of the order of the Taylor length λ. It is further reported that the distribution function is essentially independent of the Reynolds number. Our findings in Aldudak & Oberlack (2009) as well as the present work strongly support both these conclusions (figures 2 and 9).

In a series of publications aiming to directly derive turbulent scaling laws from principles only employing the infinite series of multi-point-correlation (MPC) equations Oberlack has shown (Oberlack 1999, 2000, 2001) that Lie symmetries are the essential basis for scaling laws in turbulence. In the frame work of Lie symmetry theory these special solutions are called invariant solutions. In the latter publications he showed that in canonical geometries, e.g. in channel flows, large-scale quantities, such as the logarithmic law of the wall, are exact solutions of the MPC equations.

Only recently (see Oberlack & Rosteck 2010) have these ideas been considerably extended due to the discovery that the MPC equations admit an even wider set of symmetries compared to the set of groups which are implied from the original set of equations, i.e. the Euler and Navier–Stokes equations. Specifically, a new scaling group and translational groups of the correlation tensors of all dependent variables have been discovered. These new statistical groups have important consequences for our understanding of turbulent scaling laws, which may be revealed by two examples. First, it has been demonstrated that the log-law fundamentally relies on one of the new translational groups. Further, with these new symmetries at hand all higher MPCs, which include classical one-point quantities such as the turbulent stresses, may be derived. Second, it was demonstrated that the recently discovered exponential decay law of isotropic turbulence generated by fractal grids (see Hurst & Vassilicos 2007; Seoud & Vassilicos 2007) is only admissible with the new statistical scaling symmetry.

https://doi.org/10.1017/jfm.2011.549 Published online by Cambridge University Press

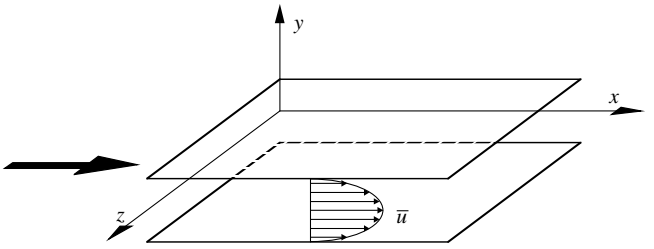


FIGURE 1. Sketch of the channel flow geometry.

—	Re_τ	L_x/h	L_z/h	$N_x \times N_y \times N_z$	Δx^+	Δz^+	Δy_c^+
Case 1	180	2π	π	$512 \times 257 \times 256$	2.2	2.2	2.2
Case 2	360	2π	π	$512 \times 257 \times 256$	4.4	4.4	4.4

TABLE 1. Simulation parameters. L_x and L_z are the streamwise and spanwise dimensions of the computational box normalized by the channel half-height h. Δy_c^+ is the dimensionless wall-normal resolution in the centre of the channel.

In particular, the latter result of an exponential decay cannot be derived from the two classical scaling groups implied by the fundamental equations of fluid motion, which has dictated our understanding of turbulence decay since the early 1930s, as implicated by the von-Kármán–Howarth equation.

The latter findings of new statistical Lie symmetry groups for the MPC have finally been derived by employing commutator theory and generating three more sets of symmetries. Together with the known symmetries of Euler and Navier–Stokes equations this finally forms a Lie algebra (Rosteck & Oberlack 2011). These results will formally be applied to DE.

In order to apply Lie symmetry theory to the DE approach, we consider the case of a turbulent pressure-driven channel flow for which a broad variety of scaling laws have been derived in the above-mentioned literature. For its validation, here we employ direct numerical simulations of turbulent channel flow at two different Reynolds numbers to analyse the geometrical statistics of the DEs (table 1). The viscous sublayer contains 20 grid points in case 1 and 14 grid points in case 2.

Figure 1 illustrates the geometry and the coordinates of the channel flow.

The paper is organized as follows: after the brief introduction to the theory of the dissipation element method and turbulent length scales in general that has been given above, the numerical simulations will be described. In § 2 the numerical method and the underlying governing equations are shown. Lie symmetry analysis of the DE distribution is presented in § 3 where we derive and validate scaling laws for DEs in turbulent channel flow. A log-normal probability density model for the DE length is introduced in § 3.3. Finally, in § 3.4 mean scalar differences of kinetic energy conditioned on element length are discussed.

https://doi.org/10.1017/jfm.2011.549 Published online by Cambridge University Press

2. Governing equations and numerical method

We investigate a pressure-driven incompressible turbulent channel flow employing the Navier–Stokes equations in the dimensionless form

$$\frac{\partial \boldsymbol{u}}{\partial t} + (\boldsymbol{u}\cdot\boldsymbol{\nabla})\boldsymbol{u} = -\boldsymbol{\nabla} p + \frac{1}{Re_\tau}\nabla^2\boldsymbol{u}, \tag{2.1}$$

$$\boldsymbol{\nabla}\cdot\boldsymbol{u} = 0, \tag{2.2}$$

where $\boldsymbol{x}$, t, $\boldsymbol{u}$ and p are respectively the position vector, time, the velocity vector and pressure. All quantities have been non-dimensionalized by the channel half-width h and the friction velocity $u_\tau = \sqrt{\tau/\rho}$ where τ is the mean wall friction, ρ is density and $Re_\tau = u_\tau h/\nu$ is the friction-based Reynolds number. The no-slip and impermeable wall boundary conditions at both channel walls are $\boldsymbol{u}(x, y = \pm h, z) = 0$. In the homogeneous streamwise (x) and spanwise (z) directions periodic boundary conditions are applied and the pressure gradient in the x-direction that drives the flow is fixed to -1. The velocities in the streamwise, wall-normal and spanwise directions are respectively denoted by $\boldsymbol{u} = (u, v, w)$.

The numerical code employed here uses well-established highly accurate spectral methods to solve the three-dimensional time-dependent incompressible Navier–Stokes equations and was developed at KTH, Stockholm (for details see Lundbladh *et al.* 1999; Skote 2001). The code adopts a spectral method with Fourier decomposition in the streamwise and spanwise directions and discretization with Chebyshev polynomials in the wall normal direction. Apart from the wall-normal integration the numerical method is similar to the one used by Kim, Moin & Moser (1987). Time integration is performed using a third-order Runge–Kutta scheme for the advective and forcing terms and second-order Crank–Nicolson for the viscous terms. The transformation between physical and spectral space is done by fast Fourier transform (FFT).

3. Symmetry analysis of the dissipation element distribution

Since in the past DE have primarily been investigated in homogeneous flows, we focus here on the question of how the DE statistics change in wall-dominated shear turbulence. For this purpose we separate the channel flow in three different layers, i.e buffer region, logarithmic region and channel core region. Though a clear-cut limit between layers is somewhat arbitrary, we adopt the following classification:

(a) buffer region: $5 < y^+ < 30$;

(b) log. region: $y^+ \geqslant 30$, $y/h < 0.3$;

(c) core region: $0.3 \geqslant y/h < 1$;

where $y^+ = yu_\tau/\nu$. Note that the viscous sublayer has been excluded from the analysis below in order to avoid ambiguity of the DE definition at the wall.

3.1. *Lie symmetries and their invariants in the channel flow*

In order to comprehend the scaling properties of the DE p.d.f., we should first reconsider the scaling symmetries of the Navier–Stokes, or rather, the Euler equations. In the large-Reynolds-number limit the Navier–Stokes equations (2.1) and (2.2) admit the two independent transformation groups of scaling

$$T_1 : t^* = t, \quad \boldsymbol{x}^* = \mathrm{e}^{a_1}\boldsymbol{x}, \quad \boldsymbol{u}^* = \mathrm{e}^{a_1}\boldsymbol{u}, \quad p^* = \mathrm{e}^{2a_1}p, \tag{3.1}$$

$$T_2 : t^* = \mathrm{e}^{a_2}t, \quad \boldsymbol{x}^* = \boldsymbol{x}, \quad \boldsymbol{u}^* = \mathrm{e}^{-a_2}\boldsymbol{u}, \quad p^* = \mathrm{e}^{-2a_2}p, \tag{3.2}$$

https://doi.org/10.1017/jfm.2011.549 Published online by Cambridge University Press

where $a_1, a_2 \in \mathbb{R}$ are independent group parameters. These transformations refer to symmetry groups, meaning that their substitution into the Navier–Stokes equations (2.1) and (2.2) (in the limit $1/Re_\tau \to 0$) leads to identical equations written in the new variables denoted by the asterisk.

Apart from the latter two groups, the Euler and Navier–Stokes equations admit the group of translation, i.e. any shift of origin leaves these equations unchanged. The corresponding transformation reads

$$T_3 : t^* = t, \quad \boldsymbol{x}^* = \boldsymbol{x} + \boldsymbol{a}, \quad \boldsymbol{u}^* = \boldsymbol{u}, \quad p^* = p, \tag{3.3}$$

and, as is apparent, this is also a symmetry transformation. A complete list of all symmetries of the Euler and Navier–Stokes equations is given in Oberlack (2000).

It is in particular the above two scaling groups, (3.1) and (3.2), and their combinations that form the basis for many turbulent scaling laws in group theory, called invariant solutions (see e.g. Oberlack 1999, 2000, 2001; Oberlack & Rosteck 2010; Rosteck & Oberlack 2011).

This is true both for small-scale turbulence and the Kolmogorov law (see Ünal 1994), as well as for scaling laws of large-scale quantities such as of wall-bounded shear flows. In particular, for a turbulent channel flow it has been shown in Oberlack (2000, 2001) that, both for the log region and for the algebraic law in the core region, scaling of space according to T_1 with the group parameter a_1 is the key property. In respect to their scaling properties the two cases are distinguished by the scaling of time T_2.

This may best be observed by reconsidering the invariant surface condition for the mean velocity for wall-bounded plane shear flows which has the form

$$\frac{\mathrm{d}y}{a_1 y + a_3} = \frac{\mathrm{d}\bar{u}}{(a_1 - a_2)\bar{u} + a_4} \tag{3.4}$$

(see Oberlack 2001). Apparently, for the log-law we have $a_2 = a_1$ while for the algebraic law we have $a_2 = n a_1$ for a fixed given value of n. Regardless of which mean-flow scaling law is active in the respective flow regime, we always have a scaling of space in the wall-normal direction according to (3.1)

$$y^* = \mathrm{e}^{a_1} y \tag{3.5}$$

which is in fact true for all length scales. Therefore, this is also valid for the length scale of the DE

$$l^* = \mathrm{e}^{a_1} l \tag{3.6}$$

where l is the Euclidian length of the DE .

From (3.3) we also obtain the translational group for y

$$y^* = y + a_3, \tag{3.7}$$

which will be employed subsequently.

For the analysis of the DE statistics Wang & Peters (2006) introduced the p.d.f. or, respectively, the conditional p.d.f. as the main quantity. In the homogeneous flow which was investigated therein the p.d.f. is only a function of the DE length, Reynolds number and perhaps a time scale ratio between turbulent and shear time scales.

For the present flow case, any statistical quantity depends on the wall normal distance y and the Reynolds number Re_τ as parameters, and hence the formal p.d.f. for

https://doi.org/10.1017/jfm.2011.549 Published online by Cambridge University Press

the length-scale distribution is of the form

$$P(l; y, Re_\tau) \tag{3.8}$$

where the Euclidean length l is now referring to the sample space variable.

The usual p.d.f. normalization condition

$$\int_0^\infty P \,\mathrm{d}l = 1 \tag{3.9}$$

together with the length-scale scaling (3.6) implies a scaling of the p.d.f. of the form

$$P^* = \mathrm{e}^{-a_1} P. \tag{3.10}$$

Further, defining the mean or expectation value for the DE

$$l_m = \int_0^\infty lP \,\mathrm{d}l \tag{3.11}$$

we instantly obtain the scaling

$$l_m^* = \mathrm{e}^{a_1} l_m. \tag{3.12}$$

At this point we invoke the two key assertions of Lie symmetry theory.

(*a*) Any concatenation of two or more symmetry groups of a given problem or differential equation is again a symmetry group. However, it is now a multi-parameter symmetry group. For example from (3.1) and (3.2) we obtain the multi-parameter group $T_{1,2} : t^* = \mathrm{e}^{a_2} t, \boldsymbol{x}^* = \mathrm{e}^{a_1} \boldsymbol{x}, \boldsymbol{u}^* = \mathrm{e}^{a_1 - a_2} \boldsymbol{u}, p^* = \mathrm{e}^{2(a_1 - a_2)} p$, which, implemented in (2.1) and (2.2), constitutes a symmetry group.

(*b*) Any invariant under a given group, i.e. a quantity which does not change form under a given symmetry group, may allow a reduction of parameter space. For example the quantity $\tilde{\boldsymbol{u}} = \boldsymbol{u}t$ is an invariant with respect to the symmetry (3.2) since its implementation in the latter leads to $\tilde{\boldsymbol{u}} = \boldsymbol{u}t = \boldsymbol{u}^* t^* = \tilde{\boldsymbol{u}}^*$. These properties of groups are in fact also true for any combination of symmetry groups. These may be invoked as new independent variables, which then lead to invariant solution under the above scaling group, often denoted similarity solutions.

With these assertions in mind, we may now construct the invariant solution of the DE p.d.f. by using (3.6), (3.10) and (3.12) to obtain the invariants $\tilde{l} = l/l_m$ and $\tilde{P} = l_m P$. Solving for P yields the invariant solution

$$P = \frac{\tilde{P}\left(\dfrac{l}{l_m}\right)}{l_m}. \tag{3.13}$$

Here, however, the y dependence is still hidden and we should now consider the combined scaling and translational group of y, i.e. (3.5) and (3.7), in conjunction with the same scaling for l_m, namely (3.12). With this we obtain the invariant form of l_m

$$l_m \sim y + c \tag{3.14}$$

where the constant c emerged due to the combined group parameters a_1 and a_3. With this at hand, we derive the alternative form of the p.d.f. scaling law (3.13) given by

$$P = \frac{\tilde{P}\left(\dfrac{l}{y + c}\right)}{y + c}. \tag{3.15}$$

https://doi.org/10.1017/jfm.2011.549 Published online by Cambridge University Press

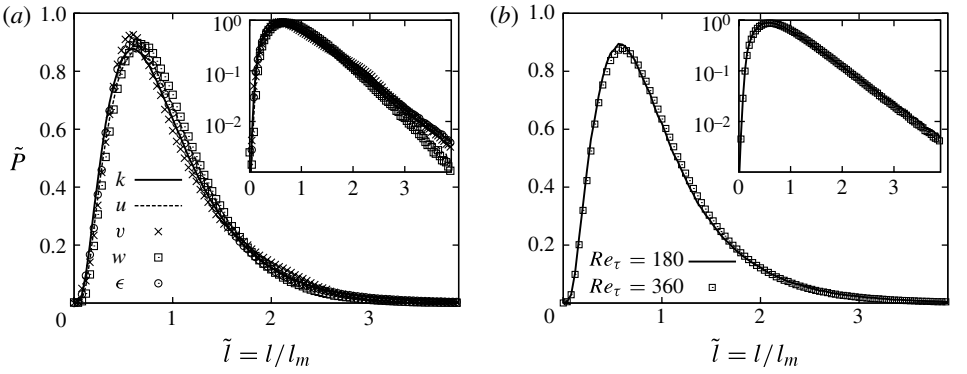


FIGURE 2. Comparison of the overall p.d.f. of the entire channel for different (a) scalars for $Re_\tau = 360$, and (b) Re_τ for scalar k.

A complete derivation of the present theory based on the key quantities of Lie theory such as infinitesimal transformations, invariant surface condition, etc. is given in Appendix.

3.2. *Validation of the dissipation element scaling laws*

Before investigating the above new scaling laws in detail, we first (a) examine the DNS data in table 1 with respect to isotropy or anisotropy of the DE p.d.f. and, in a second step (b), the Reynolds-number dependence of the DE p.d.f. To understand both the issues (a) and (b), figure 2 illustrates the marginal probability densities $\tilde{P}(l/l_m)$ of the Euclidean length of the DE of the entire channel, where the investigated scalar fields are the turbulent kinetic energy k, its dissipation rate ϵ, and the fluctuations of the velocity components (u, v, w) at two different Reynolds numbers (Re). Here, the p.d.f.s have been properly normalized using (3.9), and all length scales are rescaled by the mean length l_m for the entire channel, according to (3.11).

The distribution of the p.d.f.s is essentially log-normal as it will be shown further below. The curves show a very steep algebraic rise with an increase of the element size for small DE for all cases, and an exponential decay for larger elements after reaching a maximum at around $l \approx 0.6 l_m$. Hence, the highest probability for length scales of DE is, as to be expected, in the order of the mean length.

Related to the issue (a) of isotropy/anisotropy above, it is also interesting to note that the curves for all five scalars have remarkably coinciding shapes. From the linear plot in figure 2(a), particularly, matching curves are observed for k, u and ϵ. However, for the large length scales, taken from the semi-log subplot, it appears that u and w are closer together and apparently decay faster than the p.d.f. for k, v, and ϵ. Albeit small, the p.d.f. of the wall-normal velocity component v shows a relatively noticeable deviation from other distributions. Still, a remarkable insensitivity related to the choice of the scalar variable is observed, implying a large degree of DE isotropy which is in fact true for small as well as for large scales of DE.

An even more remarkable insensitivity with respect to different Re may be taken from figure 2(b). Curves from both Re almost perfectly coincide. This is unexpected, since both Reynolds numbers, $Re_\tau = 180$, and $Re_\tau = 360$, while relatively low, are still a factor of two apart.

Below, we intend to validate the scaling laws (3.13) and (3.14) or respectively (3.15) with the channel flow DNS data. To this end, we focus on the region of validity of

https://doi.org/10.1017/jfm.2011.549 Published online by Cambridge University Press

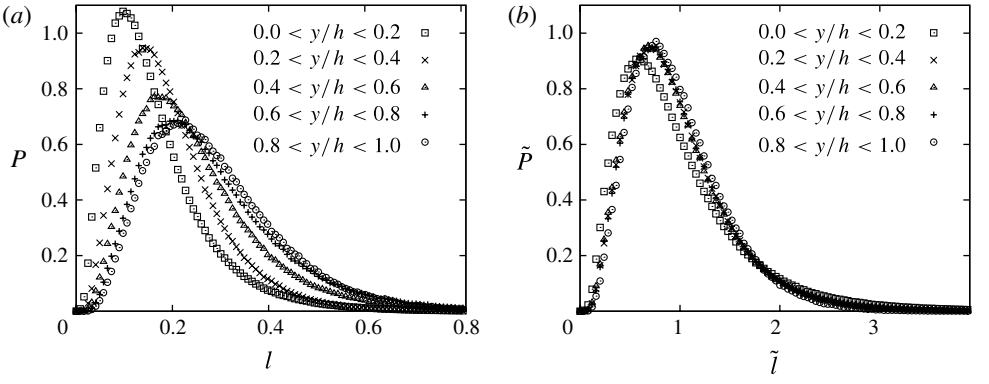


FIGURE 3. Comparison of p.d.f.s for equidistant wall-normal layers for k at $Re_\tau = 360$, where in (a) l is not normalized while in (b) l is normalized with l_m.

the above scaling laws, i.e. the log region and the algebraic region in the core of the channel. Therein, we rescale the data for the logarithmic and core regions, and plot them according to the rescaled p.d.f. $\tilde{P} = \tilde{P}(\tilde{l})$ in (3.13). In order to properly accentuate this behaviour, we split the channel into five equidistant wall-normal layers with an increment of 0.2 in the normalized wall distance y/h.

Figure 3 illustrates the p.d.f.s for the five adjacent layers, beginning with the centre, and including the most wall adjacent layer. While in figure 3(a) the p.d.f. P is only normalized according to (3.9), in figure 3(b) the length scale has also been normalized by the corresponding local mean length l_m. In other words, we plot the similarity variable $\tilde{P}$ from (3.13).

When the length scale l is not normalized, figure 3(a) indicates distinctive differences of the p.d.f.s with respect to the distance to the wall. Larger elements are seen to be located preferentially in the far-wall layers, as indicated by the p.d.f. for the core region where the maximum peak is shifted to larger elements. This is consistent with the findings in figure 4 where the mean DE length l_m is plotted against the wall-normal distance. Its linear rise in layers away from the wall is an indication of their wider spectrum of length scales compared to regions closer to the wall, where the shape of the p.d.f. becomes narrower.

In contrast to this, normalization with l_m induces a merging of the curves, especially for the region $0.2 \leqslant y/h < 1.0$. Therein, all curves nicely collapse, giving a strong indication of the invariant solution derived in § 3.1. The p.d.f. for the layer most adjacent to the wall is noticeably different from the others due to the influence of the solid walls.

For a more detailed analysis of the p.d.f.s, we investigate their behaviour in the distinguished characteristic channel flow layers mentioned above. Again, we use for the normalization of the length scale the corresponding local mean length l_m of the current layer according to (3.13). Figures 7 and 8 show the remarkable collapse of the p.d.f.s for the logarithmic layer and the core region of the channel, while the curve for the buffer region, which is closer to the wall, is shifted to the left together with its maximum peak. This layer contains more elements that are smaller than its local mean length scale compared to the layers beyond $y^+ = 30$. This behaviour can be traced back to the significant deviation from the linear scaling of the mean DE length given in figure 4, which only exhibits its validity in a restricted region.

https://doi.org/10.1017/jfm.2011.549 Published online by Cambridge University Press

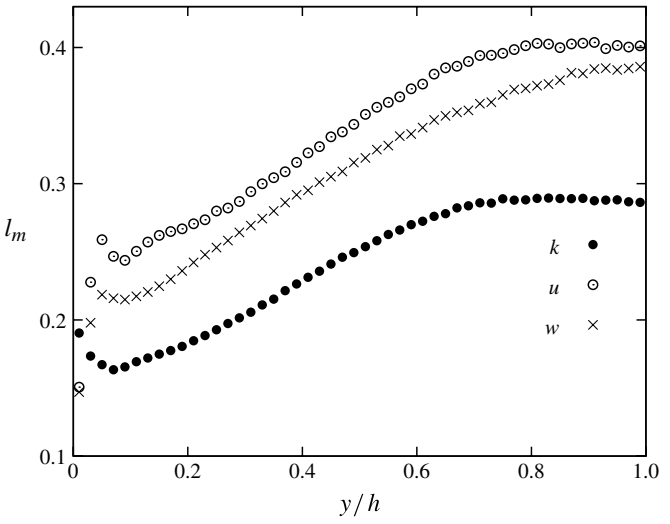


FIGURE 4. Mean length l_m of DE varying with the wall-normal direction y for $Re_\tau = 360$.

In detail, in figure 4 we observe a region with a clear linear relation between l_m and y as represented by (3.14). Though the latter is part of the basis for the p.d.f. scaling laws (3.13) or rather (3.15), we also see that the linear scaling is only confirmed in a region excluding the very centre region of the channel and, of course, the near-wall region.

Interestingly, the centre part behaviour implies a remarkable result, as it gives rise to an extended similarity behaviour for $\tilde{P}(\tilde{l})$. The reason is that, since similarity is clearly observed for all regions between $0.2 \leqslant y/h \leqslant 1.0$ in figure 3(*b*), even for the very centre layer, this is not directly supported by the finding in figure 4 in connection with the scaling laws (3.13) or (3.15). Since (3.13) or (3.15) are based on the linear scaling relating l_m and y, one would expect a clear visible deviation for the p.d.f. in the very centre layer, though only a tiny variation from the p.d.f.s taken outside the central region is detected.

Other than classical length scales such as the integral, Taylor or Kolmogorov length scale, which merely estimate turbulent scales, DEs are space filling and, in fact, have a clear geometric definition of a three-dimensional structure. This fact will subsequently be employed to estimate the number of DE, N, as a function of the wall distance y. For this, we utilize the linear scaling between l with y and take the rather simplifying assumption that DEs fill cubic sub-volumes as shown in figure 5. From this figure we may take as a first step the relation between the nth element and the distance to the wall which is a geometric series

$$2^n - 1 \sim y + c. \tag{3.16}$$

Now, in a second step, counting the number of elements at the position n we arrive at the number of DEs

$$N \sim 2^{2n}, \tag{3.17}$$

where the proportionality factor is measure of the channel size. Combining (3.16) and (3.17), we find the scaling relation

$$N(y) = \frac{b}{(y+a)^2}, \tag{3.18}$$

https://doi.org/10.1017/jfm.2011.549 Published online by Cambridge University Press

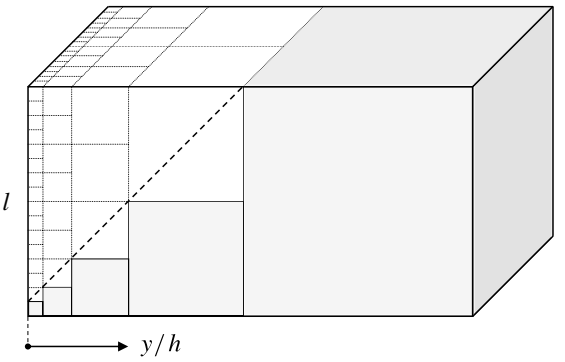


FIGURE 5. Sketch of the DEs in a turbulent channel flow approximated as cubes.

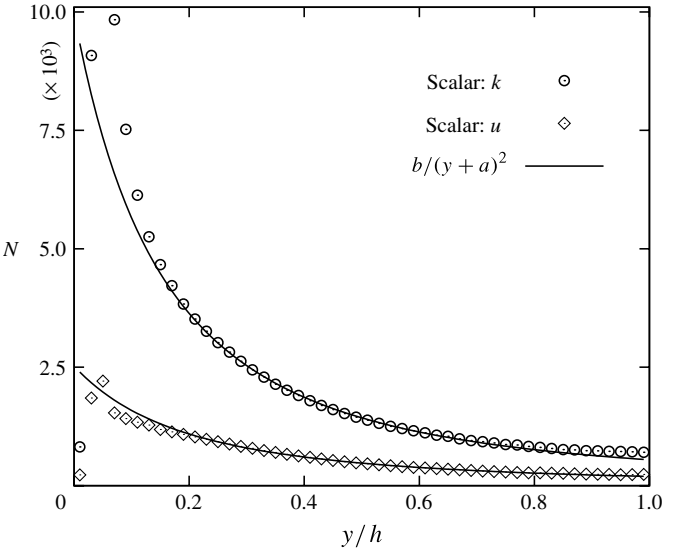


FIGURE 6. Number N of DEs as function of the wall-normal direction y for $Re_\tau = 360$.

where a and b are constants which are at most functions of Re_τ. This scaling law is nicely validated in figure 6. Weak deviations are only visible in the near wall region and in the very centre of the channel, where the linear scaling is excluded anyway as is observed in figure 4.

As pointed out above, the length of a dissipation element is defined by the Euclidean length between adjacent minimal and maximal points. Hence, saddle points are not taken into account, though these, too, are critical points with $\nabla\phi = 0$. Though simple relations between minimal, maximal, and saddle points exist for one and two dimensions, no simple counting relations exist in three dimensions, not even for Morse fields (see Peters & Wang 2006). Hence, only statistical measures may be invoked to count critical points for the present three-dimensional flow problem. In fact, the DNS data clearly indicate that the numbers of minimal and maximal points are identical. Additionally, they are indistinguishable from the number of DEs as plotted in figure 6. Hence, any further analysis of the distribution of these points is omitted. We finalize the analysis of DEs in a turbulent channel flow by investigating the link between

https://doi.org/10.1017/jfm.2011.549 Published online by Cambridge University Press

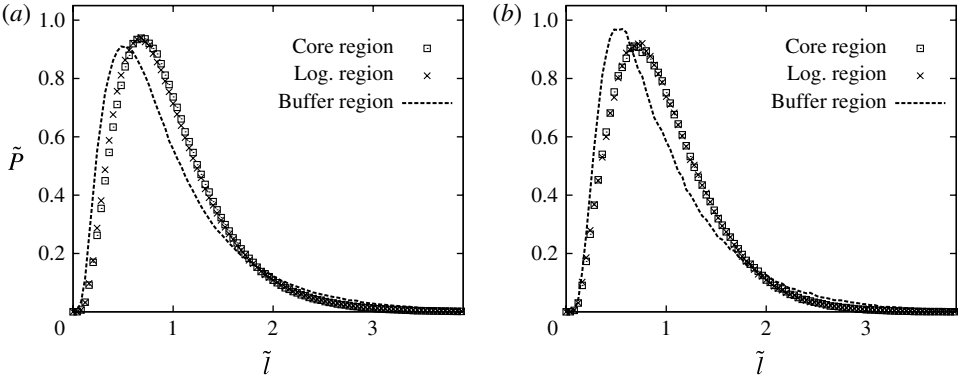


FIGURE 7. Case 2. Normalized length scale distribution function from DNS data for the fluctuations of (*a*) the turbulent kinetic energy k and (*b*) streamwise velocity component u for $Re_\tau = 360$.

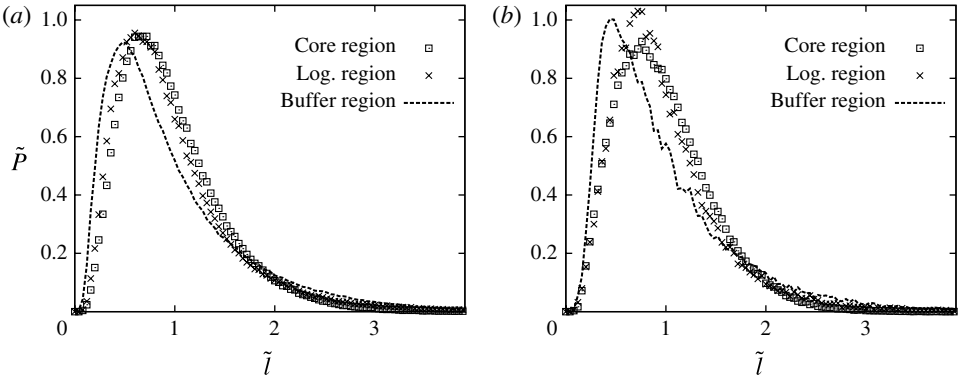


FIGURE 8. Case 1. Same as in figure 7, but with $Re_\tau = 180$.

classical length scales, in particular the Taylor length scale, and the length of the DEs. A first estimate in this respect was given in Peters & Wang (2006) where it was concluded that the expectation value of the DE distribution is proportional to the Taylor length scale, i.e.

$$l_m \sim \lambda, \tag{3.19}$$

specifying a link to classical turbulent length scales. In order to validate this conclusion, we plot the ratio l_m/λ as a function of the wall-normal direction (figure 9). This nicely reveals that – especially in the higher Re case – for a large portion of the channel height the mean length l_m scales very well with the Taylor length scale λ, substantiating the above relation (3.19).

Nevertheless, on approaching the wall this feature seems to vanish, such that the near-wall viscous and buffer layers are excluded. The lower Re case is in reasonable, but less, agreement with these findings, and low-Re effects are clearly noticeable. The figure shows that for the k scalar field DE are two times bigger than the Taylor length, whereas for the velocity component u the factor is three. This is in good agreement with Wang & Peters (2008).

https://doi.org/10.1017/jfm.2011.549 Published online by Cambridge University Press

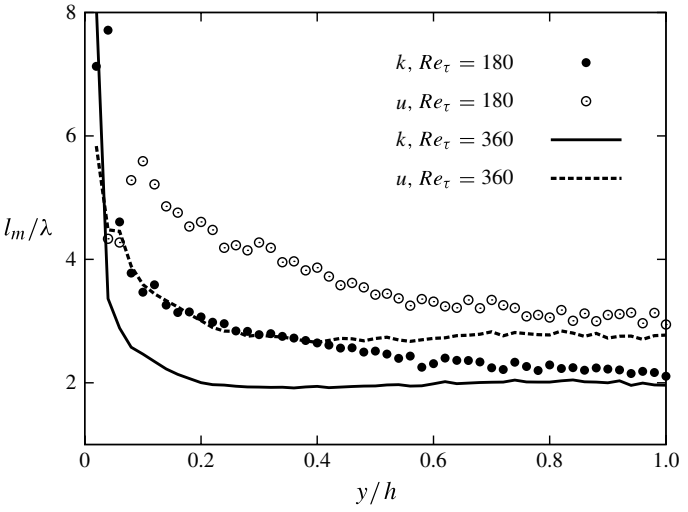


FIGURE 9. Ratio of the mean DE length l_m and Taylor length scale λ as a function of the channel height.

Further it is important to note how the plots for the same scalar but different *Re* approximate each other towards the channel centre. This coincides with the fact that the channel core region is the one most insensitive to the *Re* effects. It is to be expected that for higher *Re* both curves collapse at least for the channel core region, which is the subject of future analysis.

3.3. *Log-normal p.d.f. model*

As already noted above, the p.d.f.s of DE length reveal a skewed distribution rather than a bell-shaped, symmetrical Gaussian distribution. In a characteristic manner, skewed distributions point out non-negative values and large variances. A typical skewed distribution is the log-normal distribution, which fits the probability density of various processes in nature. A random process is log-normally distributed, by definition, if its logarithm agrees with the Gaussian distribution. Hence, all values are positive and the curve of the p.d.f. is shifted to the left.

The log-normal p.d.f. of a random variable, here ℓ, is described as

$$P(\ell) = \frac{1}{\ell\sigma\sqrt{2\pi}} \exp\left(-\frac{(\ln(\ell) - \mu)^2}{2\sigma^2}\right), \quad \ell > 0, \tag{3.20}$$

where the parameters μ and σ are a measure of the expectation value and the variance, respectively, and specify the shape of the p.d.f.

Under these conditions, let us now examine the relation between DE length and log-normal probability densities. As evident from figure 10, DE p.d.f.s closely fit the log-normal distribution. In figure 10(*a*) overall p.d.f.s of different scalar variables are displayed in a semi-logarithmic plot together with the log-normal fit for the scalar ϵ as an example. First of all, the picture emphasizes that the DE p.d.f. closely follows a log-normal distribution. Minor deviations are only visible towards the origin, where the element size is small. Upon logarithmic scaling of the horizontal axis, a second important aspect makes itself apparent. All DE p.d.f.s follow the symmetrical, normal distribution of the log-normal p.d.f., limited deviations notwithstanding.

https://doi.org/10.1017/jfm.2011.549 Published online by Cambridge University Press

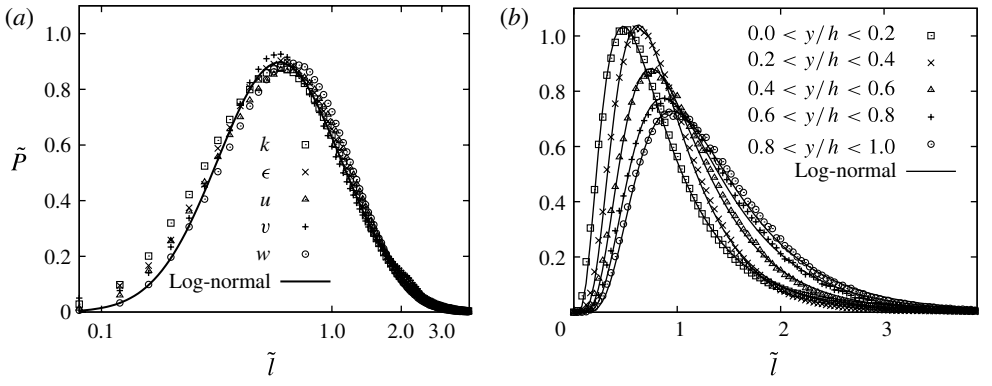


FIGURE 10. (*a*) Overall p.d.f. of different scalar variables in semi-log plot; (*b*) p.d.f. of ϵ of equidistant wall-normal layers with related log-normal fit. $Re_\tau = 360$

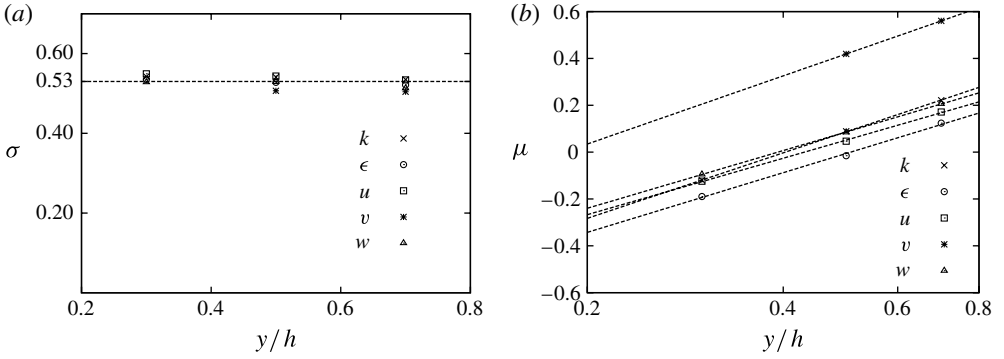


FIGURE 11. Shape parameters σ and μ as functions of y/h.

The example in figure 10(*b*) shows p.d.f.s of equidistant wall-normal layers for ϵ, highlighting an almost perfect fit by means of log-normal p.d.f.s. Adjusting the two shape parameters σ and μ, the p.d.f. can be fitted properly for the respective wall-normal layer. As a result, we examine whether these shape parameters can be written as functions of y/h. This allows us to derive a simple log-normal model which is also a function of the distance from the wall and, thus, accounts for the known wall-normal dependence of the DE p.d.f.

In figure 11(*a*,*b*) parameters σ and μ are plotted against the wall distance y/h. Note that these analytical relations again exclude the near-wall and the channel core region. While σ seems to remain constant throughout this range and again remarkably independent of the choice of the scalar quantity, μ reveals a clear logarithmic dependence on y/h. Both parameters can be described as follows:

$$\sigma \approx 0.53, \quad \mu(y^*) = \alpha \ln(\beta y^*) \tag{3.21}$$

where $y^* = y/h$. On the other hand, α and β weakly depend on the choice of the scalar variable as listed in table 2.

With these findings at hand, we may now integrate the results from the Lie-symmetries-based theory in § 3.1 with the log-normal distribution (3.20) and the findings for σ and μ in (3.21) to finally formulate a log-normal p.d.f. model for

https://doi.org/10.1017/jfm.2011.549 Published online by Cambridge University Press

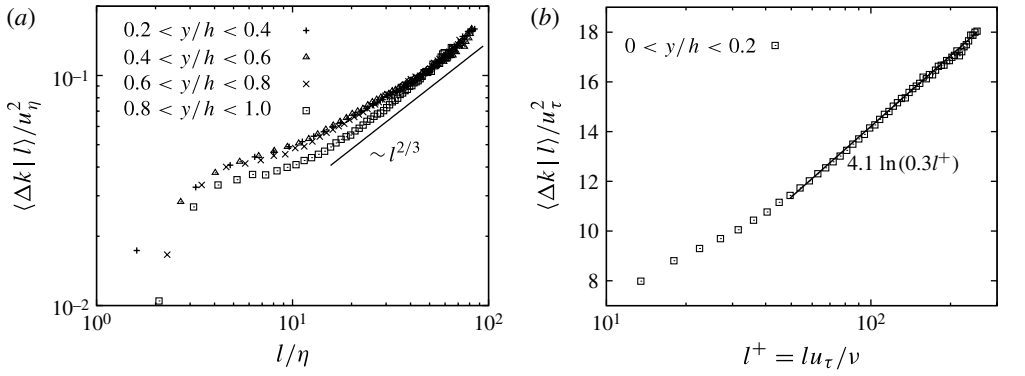


FIGURE 12. Conditional mean scalar differences for equidistant wall-normal channel layers: (*a*) logarithmic; (*b*) semi-logarithmic.

Scalar	α	β
k	0.403	2.480
ϵ	0.368	1.969
u	0.347	2.318
v	0.420	5.430
w	0.355	2.547

TABLE 2. Parameters α and β in (3.21).

the DE length depending on the wall-normal distance $y^* = y/h$,

$$P(\tilde{l}) = \frac{1}{l_m}\frac{1}{\tilde{l}\sigma\sqrt{2\pi}}\exp\left(-\frac{1}{2\sigma^2}\ln\left(\frac{\tilde{l}}{(\beta y^*)^\alpha}\right)^2\right), \quad \tilde{l} > 0. \tag{3.22}$$

3.4. *Conditional mean of scalar differences*

In this final subsection we examine the conditional mean of scalar differences between the values at the extremal points given the length of the corresponding dissipation element for the instantaneous turbulent kinetic energy k. Therefore, the first-order conditional moment is investigated to measure its scaling along the wall-normal distance. The first moment based on gradient trajectories is non-zero since the value of the turbulent kinetic energy, by definition, increases monotonically along a trajectory from the minimum to the maximum point.

Considering this, in figure 12 the conditional mean of scalar difference, non-dimensionalized with u_η^2 and u_τ^2, i.e. the Kolmogorov and the friction velocity, respectively, is plotted for five equidistant wall-normal layers.

In figure 12(*a*) we focus on the centre regions of the channel corresponding to $0.2 \leqslant y/h \leqslant 1$, where the least mean shear is present in the flow. For sufficiently large DE the double logarithmic plot reveals a power law with a scaling exponent of 2/3 which is known from Kolmogorov's hypothesis. This applies to elements whose sizes are close to the mean DE length l_m and larger ($l \geqslant l_m$).

Approaching the wall, of course, this scaling is likely to break under the influence of strong shear-induced anisotropy as can be confirmed by the semi-logarithmic

https://doi.org/10.1017/jfm.2011.549 Published online by Cambridge University Press

plot figure 12(*b*). In the near-wall layer ($0 \leqslant y/h \leqslant 0.2$) consisting of the buffer and logarithmic regions where turbulent kinetic energy scales as u_τ^2 we may invoke the same Lie symmetry arguments as for the mean velocity log-law (Oberlack 2001; Oberlack & Rosteck 2010). For this, we may rewrite the invariant equation for the mean flow (3.4) in terms of the conditional mean scalar variance

$$\frac{\mathrm{d}l}{a_1 l} = \frac{\mathrm{d}\langle \Delta k \mid l\rangle}{(a_1 - a_2)\langle \Delta k \mid l\rangle + a_5} \tag{3.23}$$

where a_1 and a_2 still refer to the scaling groups of space and time in (3.1) and (3.2), respectively, here combined to

$$t^* = \mathrm{e}^{a_2} t, \quad \boldsymbol{x}^* = \mathrm{e}^{a_1}\boldsymbol{x}, \quad \boldsymbol{u}^* = \mathrm{e}^{a_1 - a_2}\boldsymbol{u}, \quad p^* = \mathrm{e}^{2(a_1 - a_2)} p; \tag{3.24}$$

a_5, in fact, corresponds to a statistical group similar to a_4 in (3.4) (see Oberlack & Rosteck 2010).

Employing the velocity scale u_τ as the symmetry-breaking parameter for the velocity scale in (3.24), i.e. $a_1 - a_2 = 0$, we obtain from (3.23) the logarithmic scaling $\langle \Delta k \mid l\rangle = (a_5/a_1)\ln(l) + C$. Normalizing on wall coordinates yields

$$\langle \Delta k \mid l\rangle = u_\tau^2 \left(\gamma_1 \ln\left(\frac{l u_\tau}{\nu}\right) + \gamma_2 \right). \tag{3.25}$$

This is somewhat equivalent to the classical power spectrum $E(K) \sim u_\tau K^{-1}$ in the logarithmic region, where K is the wavenumber (Perry, Henbest & Chong 1986), which is nicely verified in figure 12(*b*). This logarithmic law is valid, again, for DE where $l \geqslant l_m$.

4. Conclusion

We have analysed the geometrical structure of turbulence in a turbulent channel flow employing the dissipation element approach. It has been shown that the presence of the walls has a very distinct influence on the DE statistics. On this note, the relationship between both the DE p.d.f. and the DE length, and the wall-normal direction y was investigated. Dependent on the rescaling of the p.d.f. the influence of solid walls on the length-scale distribution can be observed. Particularly, if no rescaling was employed, the p.d.f.s exhibit a strong dependence on the distance to the wall, i.e. the length-scale distribution is shifted to small scales when approaching the wall.

This distinct behaviour has been analysed by Lie symmetry group methods together with known symmetries of Navier–Stokes equations and utilized for the core region of the flow, i.e. the flow region beyond the buffer layer. Therein, the p.d.f. of the DE distribution exhibits an invariant functional form, in other words, self-similar behaviour with respect to the wall distance. This is further enhanced by the scaling behaviour of the mean DE length scale which evidences a linear scaling with the wall distance. We outlined the relationship between DE and other classical length scales and found that the DE length is proportional to the Taylor length scale for the core region of the channel.

As a further independent parameter, the Reynolds-number dependence was investigated. Here, a notable invariance is found even at the rather low Reynolds numbers of the DNS. In several other works (Benzi *et al.* 1999; Toschi *et al.* 1999; Biferale & Procaccia 2005) it has also been reported that scaling laws occur at relatively low Reynolds numbers in turbulent channel flow. In the present case

https://doi.org/10.1017/jfm.2011.549 Published online by Cambridge University Press

even anisotropy and strong shear appear to have almost no influence on the p.d.f. Performing a detailed analysis of the DNS data, the isotropy/anisotropy character of the p.d.f. as well as its dependence on the choice of the scalar variable have been investigated. It is found that all p.d.f.s collapse and hence exhibit an isotropic character. This is in strong contrast to classical Kolmogorov scaling laws which usually exhibit a strong dependence on shear and anisotropy. Both usually limit the length of the scaling law. Utilizing a geometric analogy a relation between the number of DEs and the channel distance has been formulated and validated with the statistics from DNS data.

We showed that the p.d.f.s of the DE length are essentially log-normal and derived a p.d.f. model based on the log-normal distribution. Its shape parameters have been adjusted so that the model is a function of the wall-normal distance y/h. Finally, for the conditional mean scalar differences between the extremal points of DE , it could be shown that in the centre regions of the channel Kolmogorov's 2/3 hypothesis holds whereas layers close to wall feature a logarithmic law rather than a power law.

As an outlook for DEs in other turbulent flows, the authors strongly believe that the DE p.d.f. will exhibit similar scaling behaviour, at least if canonical flows are investigated such as wakes, jets, and others. Still, the key outstanding challenge is the derivation of a DE length scale-based equation, e.g. for the p.d.f. using only Navier–Stokes equations and other first principles.

Acknowledgements

F.A. and M.O. acknowledge funding from the Deutsche Forschungsgemeinschaft (DFG) under grant number OB 96/19-1 within the research collaboration group 'Geometric structure of small-scale turbulence'.

Appendix. Lie theory for dissipations elements in wall-bounded shear flows

The starting point of Lie symmetry analysis is based on the two groups in the near-wall region of a turbulent channel flow, i.e.

(*a*) scaling group (3.5) $y^* = \mathrm{e}^{a_1} y$ which in operator form is written

$$X_1 = y\frac{\partial}{\partial y}, \tag{A 1}$$

(*b*) translation group (3.7) $y^* = y + a_3$ having the operator form

$$X_2 = \frac{\partial}{\partial y}. \tag{A 2}$$

The scaling group (A 1) together with (3.11) may be directly extended to the scaling symmetry for the DE which yields

$$X^{(l)} = y\frac{\partial}{\partial y} + l\frac{\partial}{\partial l} + l_m\frac{\partial}{\partial l_m}. \tag{A 3}$$

For the DE p.d.f. the scaling group is unknown and hence we may only assume a very general scaling group

$$X^{(P)} = nP\frac{\partial}{\partial P} \tag{A 4}$$

where n is to be specified subsequently.

https://doi.org/10.1017/jfm.2011.549 Published online by Cambridge University Press

Since Lie symmetries in infinitesimal form constitute a linear vector space we have the combined symmetry

$$X = c_1 X^{(l)} + c_2 X_2 + c_P X^{(P)} \tag{A 5}$$

where c_1, c_2 and c_P are arbitrary constants.

The determination of n may in fact be done by applying the latter invariance group to the normalization (3.9), i.e.

$$X\left[\int_0^\infty P\,\mathrm{d}l - 1\right]\Big|_{(3.9)} = 0. \tag{A 6}$$

From (A 2)–(A 5) we see that only the second part of $X^{(l)}$ and the group $X^{(P)}$ are actively operating on (A 6). With this we get

$$c_P = -c_1 \tag{A 7}$$

and hence, we obtain together with (A 5)

$$X = c_1\left[y\frac{\partial}{\partial y} + l\frac{\partial}{\partial l} + l_m\frac{\partial}{\partial l_m} - P\frac{\partial}{\partial P}\right] + c_2\frac{\partial}{\partial y}. \tag{A 8}$$

Though an explicit equation for P is not known at this point we may still construct invariant solutions. For this we apply X to the *a priori* unknown solution $P = F(l, y)$:

$$X[P - F(l, y)]|_{P-F(l,y)=0} = 0. \tag{A 9}$$

The latter is in fact a hyperbolic equation and its characteristic solution leads to the invariant surface condition in the form

$$\frac{\mathrm{d}y}{c_1 y + c_2} = \frac{\mathrm{d}l}{c_1 l} = \frac{\mathrm{d}P}{-c_1 P}. \tag{A 10}$$

The characteristics are in fact the invariants of the form

$$\tilde{l} = \frac{l}{y + c} \quad \text{and} \quad \tilde{P} = Pl. \tag{A 11}$$

Since invariants may arbitrarily be combined we can rewrite the latter to obtain the central solution (3.15)

$$P = \frac{\tilde{P}\left(\dfrac{l}{y + c}\right)}{y + c} \tag{A 12}$$

which may also be easily extended to the alternative form (3.13).

REFERENCES

ALDUDAK, F. & OBERLACK, O. 2009 Dissipation element analysis of scalar fields in wall-bounded turbulent flow. *Proceedings of EUROMECH Colloquium 512: Small Scale Turbulence and Related Gradient Statistics*, pp. 9–11.

BENZI, R., AMATI, G., CASCIOLA, C. M. & TOSCHI, F. 1999 Intermittency and structure functions in channel flow turbulence. *Phys. Fluids* **11**, 1284.

BIFERALE, L. & PROCACCIA, I. 2005 Anisotropy in turbulent flows and in turbulent transport. *Phys. Rep.* **414** (2–3), 43–164.

CORRSIN, S. 1951 On the spectrum of isotropic temperature fluctuations in isotropic turbulence. *J. Appl. Phys.* **22**, 469–473.

https://doi.org/10.1017/jfm.2011.549 Published online by Cambridge University Press

GIBSON, C. H. 1968 Fine structure of scalar fields mixed by turbulence i. Zero gradient points and minimal gradient surfaces. *Phys. Fluids* **11**, 2305–2315.

HURST, D. & VASSILICOS, J. C. 2007 Scalings and decay of fractal-generated turbulence. *Phys. Fluids* **19**, 035103.

KIM, J., MOIN, P. & MOSER, R. D. 1987 Turbulence statistics in fully developed channel flow at low Reynolds number. *J. Fluid Mech.* **177**, 133.

KOLMOGOROV, A. N. 1941 The local structure of turbulence in an incompressible viscous fluid for very large Reynolds numbers. *Dokl. Akad. Nauk SSSR* **30**, 301–305.

LUNDBLADH, A., BERLIN, S., SKOTE, M., HILDINGS, C., CHOI, J., KIM, J. & HENNINGSON, D. S. 1999 An efficient spectral method for simulation of incompressible flow over a flat plate. *Tech. Rep.* 1999:11. KTH, Stokholm.

OBERLACK, M. 1999 Similarity in non-rotating and rotating turbulent pipe flows. *J. Fluid Mech.* **379**, 1–22.

OBERLACK, M. 2000 Symmetrie, invarianz und selbstähnlichkeit in der turbulenz. Habilitation thesis, RWTH Aachen.

OBERLACK, M. 2001 A unified approach for symmetries in plane parallel turbulent shear flows. *J. Fluid Mech.* **427**, 299–328.

OBERLACK, M. & ROSTECK, A. 2010 New statistical symmetries of the multi-point equations and its importance for turbulent scaling laws. *Discret. Contin. Dyn. S.* **3** (3), 451–471.

OBUKHOV, A. 1962 Some specific features of atmospheric turbulence. *J. Fluid Mech.* **13**, 77–81.

PERRY, A. E., HENBEST, S. M. & CHONG, M. S. 1986 A theoretical and experimental study of wall turbulence. *J. Fluid Mech.* **163**, 163–199.

PETERS, N. & WANG, L. 2006 Dissipation element analysis of scalar fields in turbulence. *C. R. Mech.* **334**, 493–506.

POPE, S. B. 2000 *Turbulent Flows*. Cambridge University Press.

RICHARDSON, L. F. 1922 *Weather Prediction by Numerical Process*, p. xii+236. Cambridge University Press.

ROSTECK, A. & OBERLACK, M. 2011 Lie algebra of the symmetries of the multi-point equations in statistical turbulence theory. *J. Nonlinear Math. Phy.* **18** (suppl. 1), 251–264.

SEOUD, R. E. & VASSILICOS, J. C. 2007 Dissipation and decay of fractal-generated turbulence. *Phys. Fluids* **19**, 105108.

SKOTE, M. 2001 Studies of turbulent boundary layer flow through direct numerical simulation. PhD thesis, Royal Institute of Technology, Stockholm, Sweden.

TOSCHI, F., AMATI, G., SUCCI, S., BENZI, R. & PIVA, R. 1999 Intermittency and structure functions in channel flow turbulence. *Phys. Rev. Lett.* **82** (25), 5044–5047.

ÜNAL, G. 1994 Application of equivalence transformations to inertial subrange of turbulence. *Lie Groups Appl.* **1** (1), 232–240.

WANG, L. & PETERS, N. 2006 The length scale distribution function of the distance between extremal points in passive scalar turbulence. *J. Fluid Mech.* **554**, 457–475.

WANG, L. & PETERS, N. 2008 Length-scale distribution functions and conditional means for various fields in turbulence. *J. Fluid Mech.* **608**, 113–138.

https://doi.org/10.1017/jfm.2011.549 Published online by Cambridge University Press